Preference of Electron Transfer to Nucleophilic Addition in Reactions of Ketene Silyl Acetals with Quinones and Catalysis of Magnesium Ion

Morifumi Fujita, Shunichi Fukuzumi,* Gen-etsu Matsubayashi,* and Junzo Otera*,†

Department of Applied Chemistry, Faculty of Engineering, Osaka University, Suita, Osaka 565

†Department of Applied Chemistry, Okayama University of Science, Ridai-cho, Okayama 700

(Received November 21, 1995)

β,β-Dimethyl-substituted ketene silyl acetal (**1a**) reduces *p*-chloranil and other activated quinones with electron-withdrawing substituents to produce the carbon–oxygen adduct, the hydrolysis of which yields the corresponding hydroquinone ether. The structure of the hydroquinone ether has been determined by the X-ray crystal analysis. The reactions are significantly slowed down in benzene where the charge-transfer spectra of electron donor–acceptor complexes formed between **1a** and the activated quinones are observed. The comparison of the observed rate constant with that predicted for the electron transfer process from **1a** to *p*-chloranil indicates that the addition of **1a** to *p*-chloranil proceeds via the electron transfer from **1a** to *p*-chloranil. Although no reaction takes place between **1a** and *p*-benzoquinone, the electron affinity of which is significantly smaller than that of *p*-chloranil, the reduction of *p*-benzoquinone by **1a** occurs efficiently in the presence of magnesium ion. The kinetic expression of the Mg^{2+} catalysis changes from the first-order to second-order in $[Mg^{2+}]$ under the conditions that Mg^{2+} forms the 2 : 1 complexes with the corresponding radical anions. The catalytic effects of Mg^{2+} are approximately the same as those observed for the electron transfer reduction of these oxidants, demonstrating the important contribution of the Mg^{2+}-catalyzed electron transfer process in the addition of **1a** to *p*-benzoquinone. On the other hand, the reaction of a nonsubstituted ketene silyl acetal (**1d**) with *p*-fluoranil yields the carbon–carbon adduct rather than the carbon–oxygen adduct. The much larger rate constants of **1d** than those of **1a** despite the higher oxidation potential of **1d** suggest that the 1,2-addition to *p*-fluoranil occurs via the nucleophilic attack of **1d**, which is much less sterically hindered than **1a**, to the positively charged carbonyl carbon of *p*-fluoranil rather than an alternative electron transfer pathway.

We have recently reported that β-methyl-substitution of ketene silyl acetals increases the electron-donor ability to be becoming more susceptible to the electron transfer oxidation than the less substituted counterparts.[1,2] Another important aspect to be emphasized in relation to the novel electron transfer process is facile connection of contiguous quaternary carbon centers which still remains to be a challenging target for synthetic chemists.[3] Moreover, the electron-transfer oxidation of ketene silyl acetals and silyl enol ethers has been receiving increased attention because of its synthetic utility.[4,5] An electron transfer mechanism has recently been reported for the reduction of 2,3-dichloro-5,6-dicyano-*p*-benzoquinone (DDQ), which is known as a strong organic one-electron oxidant, by silyl enol ethers, although a nucleophilic attack of the silyl enol ether on DDQ cannot be ruled out.[6]

Such electron transfer vs. nucleophilic process alternative has been one of the central proposition in reaction mechanism.[7] In particular, extensive attention has recently been paid on the two-electron reduction of quinones by model compounds of nicotinamide adenine dinucleotide (NADH).[8—11] With regard to the reduction of quinones, magnesium perchlorate is known to act as an efficient catalyst in the reduction by NADH model compounds.[12] In this context, it has recently been disclosed that Mg^{2+} forms the 1 : 1 and 2 : 1 complexes with the radical anions of *p*-benzoquinone derivatives and that the catalytic effects of Mg^{2+} in the electron transfer reduction of *p*-benzoquinone derivatives as well as the two-electron reduction by NADH model compounds are essentially the same.[13]

This study reports our new finding on the unique electron transfer chemistry of β,β-dimethyl-substituted ketene silyl acetal (**1a**) in the addition reactions with *p*-benzoquinone and its derivatives and the novel catalytic action of Mg^{2+} ion as well as the formation of the charge transfer complexes formed between **1a** and quinones.[14] These data provide a valuable mechanistic insight into the electron transfer vs. nucleophilic dichotomy in the addition of ketene silyl acetals to quinones.

Experimental

Materials. Ketene silyl acetals ($Me_2C{=}C(OMe)OSiMe_3$ and $(Me_3Si)HC{=}C(OMe)OSiMe_3$) were purchased from Aldrich. The other ketene silyl acetals ($Me_2C{=}C(OEt)OSiEt_3$, (*E*)-$Me(H)C{=}C(OEt)OSiEt_3$, and $H_2C{=}C(OEt)OSiEt_3$) were prepared according to the literature method.[15] *p*-Benzoquinone and its derivatives were obtained commercially and purified by the standard method.[16] 2, 3-Dimethyl-2-butene was also obtained from Aldrich. Magnesium perchlorate was obtained from Nacalai Tesque. Dichloromethane, benzene, and acetonitrile used as solvents were purified and dried by the standard procedure.[16]

Reaction Procedure and Analyses. Typically, to a dichloromethane solution (1.0 cm^3) containing *p*-chloranil (0.04 mol dm^{-3}) was added $Me_2C{=}C(OMe)OSiMe_3$ (0.40 mol dm^{-3}). After the reaction was complete in 1 h, the resulting solution containing the product mixture was evaporated and dried in vacuum. The residue was dissolved in [^{2}H]chloroform ($CDCl_3$) and analyzed by ^{1}H NMR and/or ^{13}C NMR spectroscopy. The NMR measurements were performed using a Japan Electron Optics JNM-GSX-400 NMR spectrometer. The product mixtures were precipitated from concentrated solution. Hydroquinone ether **3** was isolated by the hydrolysis of **2** and then recrystallized from CH_2Cl_2.

2: ^{1}H NMR ($CDCl_3$) δ = 0.33 (s, 9H), 1.58 (s, 6H), 3.84 (s, 3H); ^{13}C NMR ($CDCl_3$) δ = 0.76 (C–Si), 24.88 ($\underline{Me}_2C$), 52.55 (O–Me), 83.77 (O–$\underline{C}Me_2$), 124.81 (aroma. C–Cl), 128.86 (aroma. C–Cl), 144.38 (aroma. C–O), 147.13 (aroma. C–O), 173.288 (C=O).

3: ^{1}H NMR ($CDCl_3$) δ = 1.58 (s, 6H), 3.85 (s, 3H), 6.17 (s, 1H); ^{13}C NMR ($CDCl_3$) δ = 24.90 ($\underline{Me}_2C$), 52.62 (O–Me), 83.85 (O–$\underline{C}Me_2$), 118.90 (aroma. C–Cl), 129.00 (aroma. C–Cl), 143.51 (aroma. C–O), 146.39 (aroma. C–O), 173.35 (C=O). Anal. Calcd for $C_{11}H_{10}Cl_4O_4$: C, 37.96; H, 2.90%. Found: C, 37.66; H, 2.72%.

4: ^{1}H NMR ($CDCl_3$) δ = 0.29 (s, 9H), 1.57 (s, 6H), 3.81 (s, 3H);

5: ^{1}H NMR ($CDCl_3$) δ = 0.38 (s, 9H), 1.62 (s, 6H), 3.84 (s, 3H); ^{13}C NMR ($CDCl_3$) δ = 1.45 (C–Si), 25.30 ($\underline{Me}_2C$), 52.50 (O–Me), 84.10 (O–$\underline{C}Me_2$), 118.85 (aroma. C–Cl), 123.20 (aroma. C–Cl), 146.98 (aroma. C–O), 149.44 (aroma. C–O), 173.62 (C=O). Anal. Calcd for $C_{14}H_{18}Br_4O_4Si$: C, 28.08; H, 3.03; Br, 53.38%. Found: C, 27.44; H, 2.95; Br, 52.61%.

6: ^{1}H NMR ($CDCl_3$) δ = 0.85 (q, 6H, J = 7.5 Hz), 0.98 (t, 9H, J = 7.5 Hz), 1.35 (t, 3H, J = 7.3 Hz), 1.57 (s, 6H), 4.29 (q, 2H, J = 7.3 Hz).

7: ^{1}H NMR ($CDCl_3$) δ = 0.65 (q, 6H, J = 7.8 Hz), 0.95 (t, 9H, J = 7.8 Hz), 1.16 (t, 3H, J = 7.3 Hz), 1.38 (d, 3H, J = 7.3 Hz), 3.45 (q, 1H, J = 7.3 Hz), 4.02 (q, 2H, J = 7.3 Hz).

8: ^{1}H NMR ($CDCl_3$) δ = 0.61 (q, 6H, J = 7.8 Hz), 0.93 (t, 9H, J = 7.8 Hz), 1.20 (t, 3H, J = 7.3 Hz), 3.20 (s, 2H), 4.11 (q, 2H, J = 7.3 Hz); ^{13}C NMR ($CDCl_3$) δ = 5.47 6.40, 13.94, 40.62, 61.50, 70.66 (t, J_{CF} = 24 Hz), 137.93 (dt, J_{CF} = 267, 7 Hz), 153.49 (dt, J_{CF} = 283, 10 Hz), 70.66 (t, J_{CF} = 24 Hz), 166.69, 172.06 (t, J_{CF} = 22 Hz); ^{19}F NMR ($CDCl_3$) δ = 132.54 (d, J_{FF} = 11 Hz), 157.65 (d, J_{FF} = 11 Hz).

Spectral Measurements. Typically, a benzene solution (3 cm^3) of 2.0×10^{-2} mol dm^{-3} *p*-chloranil contained in a 10-mm quartz cuvette was equilibrated in a cell holder of Shimadzu UV-160A spectrophotometer, which was thermostated at 298 K. As soon as the ketene silyl acetal or 2,3-dimethylbutene was added to the cuvette by means of a microsyringe, it was thoroughly mixed. With most quinone derivatives, the absorption spectra decreased within a few minutes and the rapid scan was required to obtain the reproducible initial absorption spectra (within 5% experimental errors).

Kinetic Measurements. Typically, a dichloromethane (0.4 cm^3) solution of 8.0×10^{-4} mol dm^{-3} *p*-chloranil contained in a 1-mm quartz cuvette was placed in cell holder of Simadzu UV-160A spectrophotometer, which was thermostated at 298 K. The ketene silyl acetal was added to the cuvette by means of a microsyringe, followed by the vigorous shaking. Rates of the reduction of *p*-chloranil were followed by the disappearance of the absorbance (λ = 291 nm) due to *p*-chloranil. Kinetic measurements for the fast reactions with half-lives <10 s were performed by using a Union RA-103 stopped-flow spectrophotometer. All the kinetics measurements were carried out under the pseudo-first-order conditions where the concentraions of ketene silyl acetals were maintained at greater than ten-fold excess of the concentraion of quinone derivatives. Pseudo-first-order rate constants were determined by least-squares curve fit by use of an Otsuka Electronics stopped-flow program. The pseudo-first-order plots were linear for three or more half-lives with the correlation coefficient $\rho > 0.999$.

X-Ray Crystal Structure Determination of *p*-HOC_6Cl_4-$OCMe_2COOMe$ (3). Accurate unit-cell parameters were determined from 24 reflections with 2θ values from 49 to 52° measured with a Rigaku four-circle difractometer at the Research Center for Protein Engineering, Institute for Protein Research, Osaka University. Crystal Data. $C_{11}H_{10}Cl_4O_4$, M = 348.01, monoclinic, space group $P2_1/c$, a = 15.826(2), b = 10.3295(9), c = 8.794(5) Å, β = 101.23(2)°, U = 1410.1(9) Å^3, Z = 4, $F(000)$ = 704.0, D_{calcd} = 1.639(1) g cm^{-3}, D_m (floating) = 1.63 g cm^{-3}, and μ(Cu $K\alpha$) = 77.1 cm^{-1}. Intensities were collected in the range $5 < 2\theta < 120°$ for a crystal with approximate dimensions 0.12×0.24×0.48 mm, using graphite-monochromatized Cu $K\alpha$ (λ = 1.5418 Å) radiation and the ω–2θ scan technique was used at a 2θ scan rate of 4° min^{-1} and scan width in 2θ of $(1.1+0.35\tan\theta)°$. Three check reflections were monitored after every 100 reflections. No significant variation in their intensities was observed throughout the data collection. Lorentz and polarization factors were applied and an absorption correction made.[17] Maximum and minimum transmission coefficients were 1.00 and 0.62, respectively. To avoid an appreciable extinction effect, 13 reflections with $|F_{calcd}| > 230$ were omitted from the original data. A total of 2386 unique reflections were measured, of which 2130 with $|F_o| > 3\sigma(F)$ were used for the structure determination. The structure was solved according to the direct (MULTAN) methods.[18] Subsequent Fourier maps showed the positions of all the non-hydrogen atoms, which were refined anisotropically by the block-diagonal least-squares procedure. All the hydrogen atoms were found from the difference-Fourier maps. The final refinement with anisotropic thermal parameters for the non-hydrogen atoms and isotropic parameters for the hydrogen atoms converged at R = 0.039 and R' = 0.041, using the weighting scheme $w^{-1} = \sigma^2(F_o) + 0.002F_o^2$. Atomic scattering factors used in the refinement were taken from Ref. 19.

Crystallographic calculations were performed using the programs of Professor K. Nakatsu, Kwansei Gakuin University, on an ACOS computer at the Research Center of Protein Engineering, Institute for Protein Research, Osaka University.

Results and Discussion

Addition of Ketene Silyl Acetals to Halogenated *p*-Benzoquinones. *p*-Chloranil (Cl_4Q) is readily reduced by a β,β-dimethyl-substituted ketene silyl acetal ($Me_2C{=}C(OMe)OSiMe_3$: **1a**) to yield the carbon–oxygen adduct (**2**) as shown in Eq. 1.

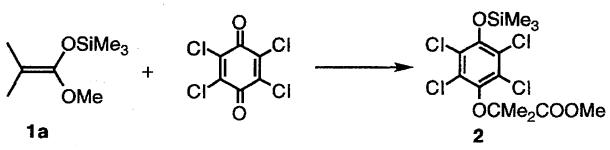

(1)

The hydrolysis of **2** yields the corresponding hydroquinone ether (**3**) quantitatively, Eq. 2.

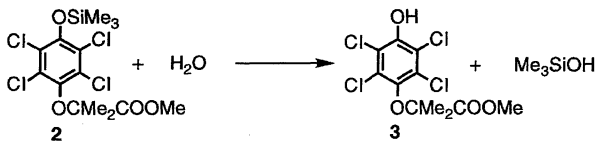

(2)

No other products such as radical coupling products of **1a** and Cl_4Q were formed. The molecular structure of **3** (Fig. 1) has been determined by the X-ray crystal analysis (the crystal data and data collection are given in Experimental). The atomic coordinates, thermal parameters, selected distances, and bond angles are listed in Tables 1, 2, and 3. Similarly, **1a** also gave the carbon–oxygen adducts (**4** and **5**) for the addition to *p*-fluoranil (F_4Q) and *p*-bromanil (Br_4Q), respectively (Chart 1). The other ketene silyl acetals ($Me_2C{=}C(OEt)OSiEt_3$; **1b** and (*E*)-$Me(H)C{=}C(OEt)OSiEt_3$; **1c**) reduce Cl_4Q to yield the carbon–oxygen adducts (**6** and **7**, respectively) as well. In contrast, the reaction of the less hindered nonsubstituted ketene silyl acetal ($CH_2{=}C(OEt)OSiEt_3$: **1d**) with F_4Q yields selectively the carbon–carbon adduct (**8**), which is identified by ^1H, ^{13}C, and ^{19}F NMR spectra (see Experimental), Eq. 3.

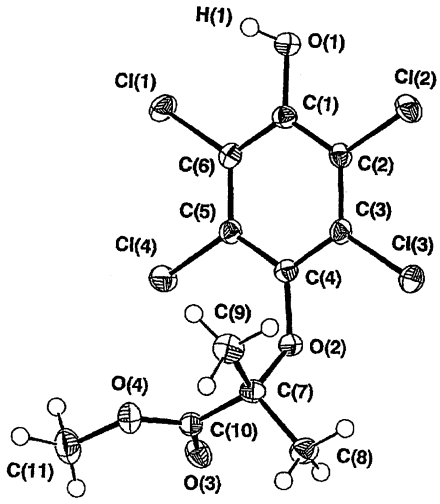

Fig. 1. ORTEP drawing of the molecular structure of **3**.

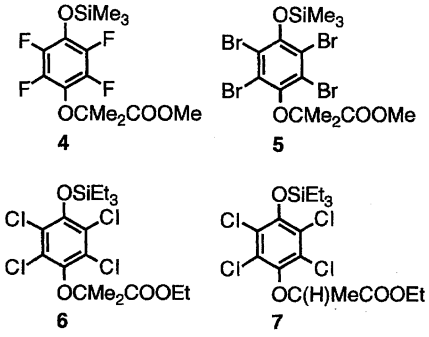

Chart 1.

Table 1. Atomic Coordinates and Temperature Factors ($B^{a)}$) for **3**, with Estimated Standard Deviations in Parentheses

Atom	*x*	*y*	*z*	*B*
Cl(1)	0.91347(5)	0.44492(9)	0.3586(1)	3.95(2)
Cl(2)	0.57146(5)	0.50116(9)	0.2116(1)	3.94(2)
Cl(3)	0.55302(5)	0.21334(9)	0.0953(1)	4.23(3)
Cl(4)	0.89566(5)	0.15616(9)	0.2521(1)	4.13(2)
O(1)	0.7463(2)	0.5817(2)	0.3286(3)	3.31(6)
O(2)	0.7158(1)	0.0739(2)	0.1261(3)	2.62(5)
O(3)	0.8283(2)	−0.1346(2)	0.1216(3)	3.52(6)
O(4)	0.8409(2)	−0.1327(3)	0.3769(3)	3.55(6)
C(1)	0.7408(2)	0.4557(3)	0.2865(4)	2.61(8)
C(2)	0.6604(2)	0.4035(3)	0.2253(4)	2.57(8)
C(3)	0.6527(2)	0.2755(3)	0.1755(4)	2.66(8)
C(4)	0.7248(2)	0.1965(3)	0.1849(4)	2.52(8)
C(5)	0.8051(2)	0.2503(3)	0.2443(4)	2.53(8)
C(6)	0.8127(2)	0.3782(3)	0.2929(4)	2.70(8)
C(7)	0.7140(2)	−0.0382(3)	0.2303(4)	2.74(8)
C(8)	0.6429(2)	−0.1261(4)	0.1475(5)	3.59(9)
C(9)	0.6984(2)	0.0019(4)	0.3870(4)	3.86(9)
C(10)	0.8004(2)	−0.1065(3)	0.2352(4)	2.78(8)
C(11)	0.9249(3)	−0.1946(4)	0.3935(6)	4.87(12)
H(1)	0.780(3)	0.590(4)	0.416(5)	3.2(10)
H(2)	0.694(2)	−0.082(4)	0.447(4)	2.2(9)
H(3)	0.742(2)	0.049(3)	0.444(4)	1.3(7)
H(4)	0.644(2)	0.047(4)	0.374(4)	1.2(7)
H(5)	0.642(2)	−0.198(4)	0.204(5)	2.3(9)
H(6)	0.650(2)	−0.143(3)	0.054(4)	2.4(7)
H(7)	0.585(3)	−0.079(5)	0.140(6)	3.4(11)
H(8)	0.947(3)	−0.214(5)	0.514(6)	6.1(15)
H(9)	0.960(3)	−0.125(5)	0.387(6)	5.9(14)
H(10)	0.923(2)	−0.259(4)	0.328(4)	1.9(7)

a) Non-hydrogen atoms are anisotropic and hydrogen atoms are isotropic.

Table 2. Bond Lengths (Å) for **3**, with Estimated Standard Deviations in Parentheses

Cl(1)–C(6)	1.728(3)	C(1)–C(6)	1.383(5)
Cl(2)–C(2)	1.715(3)	C(2)–C(3)	1.391(5)
Cl(3)–C(3)	1.723(3)	C(4)–C(5)	1.393(4)
Cl(4)–C(5)	1.721(3)	C(7)–C(8)	1.515(5)
O(1)–C(1)	1.350(4)	C(7)–C(9)	1.504(5)
O(2)–C(4)	1.365(4)	C(7)–C(10)	1.532(5)
O(2)–C(7)	1.481(4)	C(1)–C(2)	1.393(4)
O(3)–C(10)	1.204(5)	C(3)–C(4)	1.390(4)
O(4)–C(10)	1.314(4)	C(5)–C(6)	1.389(5)
O(4)–C(11)	1.454(5)		

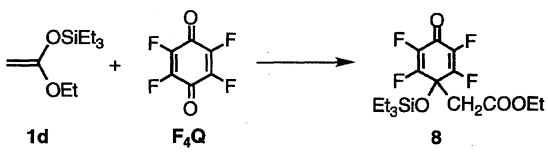

(3)

In the case of reaction of **1d** with Cl_4Q, however, both the carbon–carbon adduct (79%) and carbon–oxygen adduct (21%) were formed.

Charge-Transfer Complexes Formed between Ketene Silyl Acetal and Quinones. New broad absorption bands, which are characteristic of the charge-transfer (CT)

Table 3. Bond Angles (deg) for **3**, with Estimated Standard Deviations in Parentheses

C(10)–O(4)–C(11)	117.0(3)	O(1)–C(1)–C(2)	118.8(3)
O(1)–C(1)–C(6)	122.6(3)	C(2)–C(1)–C(6)	118.4(3)
Cl(2)–C(2)–C(1)	118.4(3)	Cl(2)–C(2)–C(3)	121.2(2)
C(1)–C(2)–C(3)	120.4(3)	Cl(3)–C(3)–C(2)	119.9(2)
Cl(3)–C(3)–C(4)	118.7(2)	C(2)–C(3)–C(4)	121.4(3)
O(2)–C(4)–C(3)	119.9(3)	O(2)–C(4)–C(5)	122.1(3)
C(3)–C(4)–C(5)	117.8(3)	Cl(4)–C(5)–C(4)	118.8(3)
Cl(4)–C(5)–C(6)	120.2(2)	C(4)–C(5)–C(6)	120.9(3)
Cl(1)–C(6)–C(1)	118.8(3)	Cl(1)–C(6)–C(5)	120.1(2)
C(1)–C(6)–C(5)	121.1(3)	O(2)–C(7)–C(8)	105.7(3)
O(2)–C(7)–C(9)	112.2(3)	O(2)–C(7)–C(10)	104.6(3)
O(2)–C(7)–C(5)	130.4(11)	C(8)–C(7)–C(9)	111.5(3)
C(8)–C(7)–C(10)	108.3(3)	C(9)–C(7)–C(10)	113.9(3)
O(3)–C(10)–O(4)	123.2(3)	C(4)–O(2)–C(7)	120.3(2)
O(3)–C(10)–C(7)	123.9(3)	O(4)–C(10)–C(7)	112.9(3)

transition,[20] are observed in the visible region immediately upon mixing a benzene solution of *p*-fluoranil (F_4Q) or the other quinone derivatives with **1a** (Eq. 4)

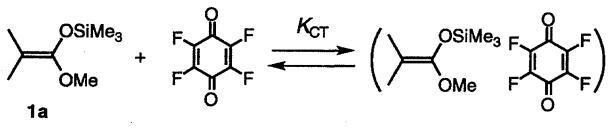

(4)

as shown in Fig. 2. Similar CT spectra were observed for electron donor–acceptor (EDA) complexes formed between 2,3-dimethyl-2-butene and quinones in benzene (Eq. 5).

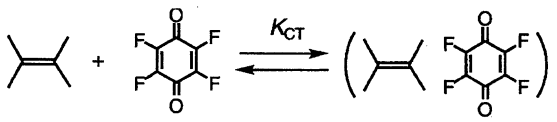

(5)

The CT absorption maxima for the EDA complexes of **1a** are significantly red-shifted relative to λ_{max} for the 2,3-dimethyl-2-butene complexes as shown in Table 4. The formation constants (K_{CT}) and the extinction coefficients (ε_{CT}) of the EDA complexes of **1a** and various quinones in benzene were determined by the classical Benesi–Hildebrand method by utilizing the absorbance change given by Eq. 6,[21]

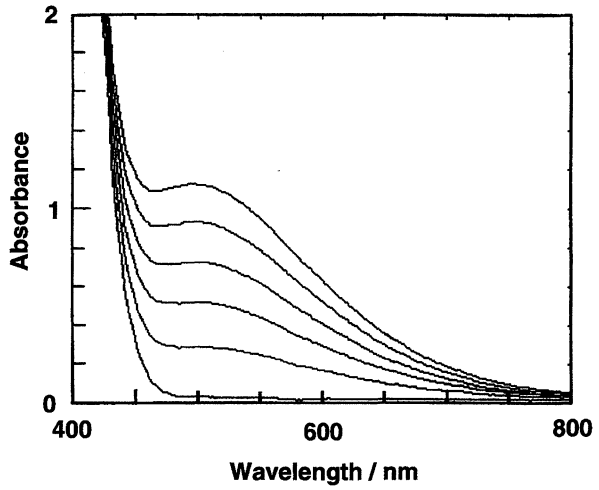

Fig. 2. The charge-transfer spectra of EDA complexes formed between **1a** (0, 0.07, 0.14, 0.22, 0.29, 0.35 mol dm^{-3}) and *p*-fluoranil (F_4Q, 3.2×10^{-2} mol dm^{-3}) in benzene at 298 K, λ_{max}=495 nm.

$$C_0/A = (K_{CT}\varepsilon_{CT})^{-1}D_0^{-1} + \varepsilon_{CT}^{-1} \quad (6)$$

where C_0 and D_0 are the initial concentrations of a quinone derivative and **1a**, respectively, in a cell of unit path length. The results in Table 4 were obtained with various amounts of **1a** in excess.

For the weak EDA complexes in which the overlap integrals between the donor and acceptor orbitals are small, the CT transition energy ($h\nu_{CT}$) can be expressed to first-order approximation as in Eq. 7,

Table 4. Formation of EDA Complexes of Quinones with $Me_2C{=}C(OMe)OSiMe_3$ in Benzene at 298 K

Quinone[a]	E^0_{red} vs. SCE/V	λ_{max} nm	$h\nu_{CT}$[b] eV	ε_{CT} dm^3 mol^{-1} cm^{-1}	K_{CT} dm^3 mol^{-1}	$\varepsilon_{CT}K_{CT}$ dm^6 mol^{-2} cm^{-1}
DDQ	0.51	c)	c) (2.17)	c)	c)	c)
DCQ	0.28	c)	c) (2.34)	c)	c)	c)
F_4Q	−0.04	495	2.50 (2.71)	176	0.66	116
Cl_4Q	0.01	510	2.43 (2.64)	260	0.25	65
Br_4Q	0.00	500	2.48 (2.61)	101	0.58	58
2,6-Cl_2Q	−0.18	477	2.60 (2.85)	84	0.34	29
2,5-Cl_2Q	−0.18	472	2.63 (2.88)	64	0.48	30
2,5-Br_2Q	—	480	2.58 (2.81)	154	0.17	26
ClQ	−0.34	440	2.82 (3.05)	d)	d)	18
Q	−0.50	e)	e) (3.26)	e)	e)	e)

a) The abbreviation of quinones: 2,3-dichloro-5,6-dicyano-*p*-benzoquinone (DDQ), 2,3-dicyano-*p*-benzoquinone (DCQ), *p*-fluoranil (F_4Q), *p*-chloranil (Cl_4Q), *p*-bromanil (Br_4Q), 2,6-dichloro-*p*-benzoquinone (2,6-Cl_2Q), 2,5-dichloro-*p*-benzoquinone (2,5-Cl_2Q), chloro-*p*-benzoquinone (ClQ), *p*-benzoquinone (Q). b) The EDA complexes of $Me_2C{=}CMe_2$ and quinones in benzene at 298 K in parentheses. c) The CT band was not observed because of rapid reduction of the quinone derivative. d) The K_{CT} value is too small to be determined accurately. e) The CT band maximum could not be determined accurately, since the CT band overlapped with the absorption band of the quinone itself.

$$h\nu_{CT} = I_D - E_A + \omega \quad (7)$$

where I_D is the ionization potential of the donor, E_A is the electron affinity of the acceptor, and ω is the interaction energy between the donor and acceptor moieties in the CT excited state.[22] The electron affinity E_A is related to the one-electron reduction potential in solution by Eq. 8,

$$E_A = E^0_{red} + C_a - \Delta G^s/F \quad (8)$$

where C_a is a constant which includes the potential of the reference electrode on the absolute scale and the junction potential,[23] ΔG^s (in kcal mol^{-1}) represents the solvation of the radical anion of the acceptor relative to the neutral acceptor, and F is the Faraday constant. Combination of Eqs. 7 and 8 gives Eq. 9,

$$h\nu_{CT} = C_b - E^0_{red} \quad (9)$$

where $C_b = I_D - C_a + \omega + \Delta G^s/F$. Provided that the solvation energy ΔG^s and the interaction energy ω are constant in a series of *p*-benzoquinone derivatives in Table 4, a linear correlation between $h\nu_{CT}$ and E^0_{red} is expected to hold with a slope of -1. In fact such a linear correlation (Eqs. 10 and 11 for **1a** and 2,3-dimethyl-2-butene, respectively) is observed in Fig. 3.

$$h\nu_{CT} = 2.45 - 1.02E^0_{red} \quad (10)$$

$$h\nu_{CT} = 2.67 - 1.09E^0_{red} \quad (11)$$

The smaller $h\nu_{CT}$ values of **1a** than 2,3-dimethyl-2-butene at the same E^0_{red} value in Fig. 4 correspond to the strong electron donor ability of **1a** relative to 2,3-dimethyl-2-butene by the replacement of two methyl groups of 2,3-dimethyl-2-butene by the more electron-donating groups, i.e., $OSiMe_3$ and OMe in **1a**.

Kinetics. Rates of the reduction of *p*-benzoquinone derivatives with large excess of ketene silyl acetals obey the ordinary pseudo-first-order kinetics. The dependence of the pseudo-first-order rate constant (k_f) on the concentration of ketene silyl acetal [**1a**] exhibits a curvature from the linear dependence (Fig. 4). Such a curved dependence of k_f on [**1a**] is consistent with the independent, spectroscopic evidence for the formation of CT complexes (vide supra) which must be accommodated in the mechanistic formulation for the reduction of *p*-chloranil by **1a** as shown in Scheme 1. If the

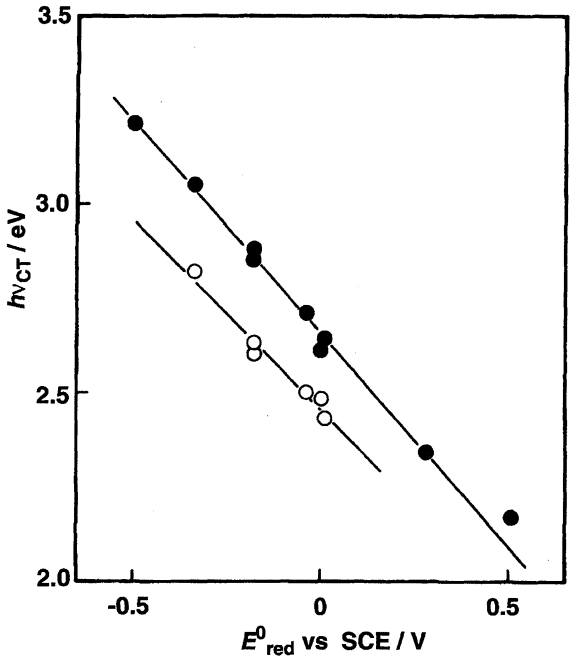

Fig. 3. Dependence of the CT transition energies ($h\nu_{CT}$) of EDA complexes of **1a** (○) and 2,3-dimethyl-2-butene (●) with quinones on the reduction potentials (E^0_{red}) of quinones.

CT complex is a precursor for the reduction of *p*-chloranil by **1a**, the k_f is expressed by Eq. 12,

$$k_f = k_1 K_{CT}[\mathbf{1a}]/(1 + K_{CT}[\mathbf{1a}]) \quad (12)$$

in which k_1 is the first-order rate constant for the reaction through the CT complex and k_2=0 in Scheme 1. Equation 12 is rewritten by Eq. 13.

$$k_f^{-1} = k_1^{-1} + (k_1 K_{CT}[\mathbf{1a}])^{-1} \quad (13)$$

The plots of k_f^{-1} vs. $[\mathbf{1a}]^{-1}$ for the reduction of *p*-chloranil and *p*-bromanil give the linear correlations as shown in Fig. 5. From the intercepts and slopes are obtained the k_1 and K_{CT} values which are listed in Table 5 together with the results for other quinones.

Alternative reaction pathway through the direct bimolecular reaction of *p*-chloranil with **1** (k_2) is also shown in Scheme 1. In such a case the CT complex is in a dead-end equilibrium. The difference lies in whether the second-order

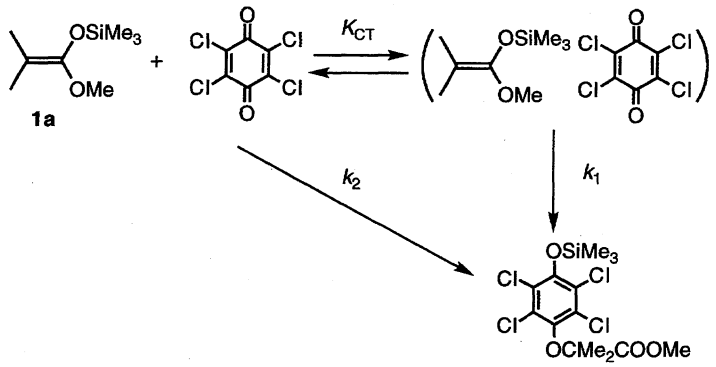

Scheme 1.

Table 5. The Kinetic Data for the Reduction of Quinones by **1a** in CH_2Cl_2 at 298 K

Quinone	E^0_{red} vs. SCE/V	[quinone] mol dm^{-3}	λ [a)] nm	k_{obsd} dm^3 mol^{-1} s^{-1}	k_1 s^{-1}	K_{CT} dm^3 mol^{-1}
o-Cl_4Q	0.14	6.5×10^{-4}	455	5.4×10^{2}	b)	b)
F_4Q	−0.04	6.3×10^{-3}	339	4.4×10^{-1}	4.0×10^{-1}	1.1
Cl_4Q	0.01	8.1×10^{-4}	291	3.5×10^{-2}	4.4×10^{-2}	0.80
Br_4Q	0.00	1.3×10^{-3}	313	7.4×10^{-3}	1.4×10^{-2}	0.53
2,6-Cl_2Q	−0.18	2.1×10^{-3}	275	1.0×10^{-2}	1.4×10^{-2}	0.70
2,5-Cl_2Q	−0.18	1.1×10^{-3}	273	1.9×10^{-3}	c)	c)
2,5-Br_2Q	—	7.5×10^{-4}	288	4.2×10^{-3}	c)	c)
ClQ	−0.34	d)	d)	d)	d)	d)
Q	−0.50	d)	d)	d)	d)	d)

a) The monitored wavelength. b) The reaction was too fast to determine K_{CT}. c) The K_{CT} value was too small to be determined accurately. d) The reaction was too slow to determine k_{obsd} accurately.

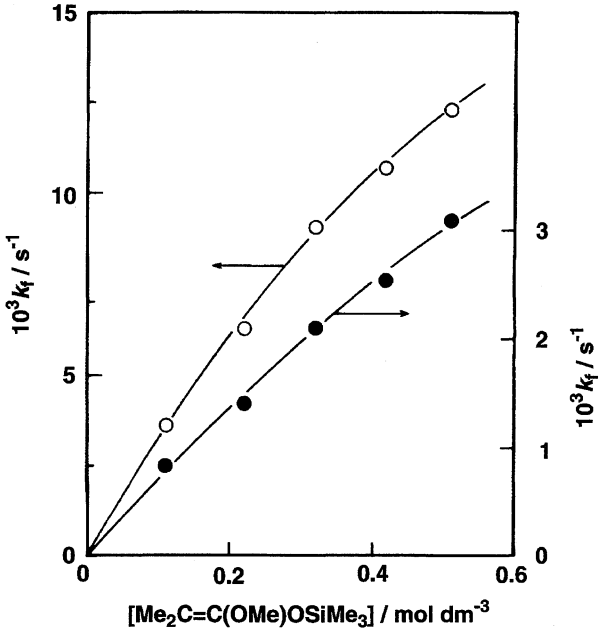

Fig. 4. Dependence of the pseudo-first-order rate constants (k_f) on [Me_2C=C(OMe)$OSiMe_3$] for the reduction of *p*-chloranil (○) and *p*-bromanil (●) by **1a** in CH_2Cl_2 at 298 K.

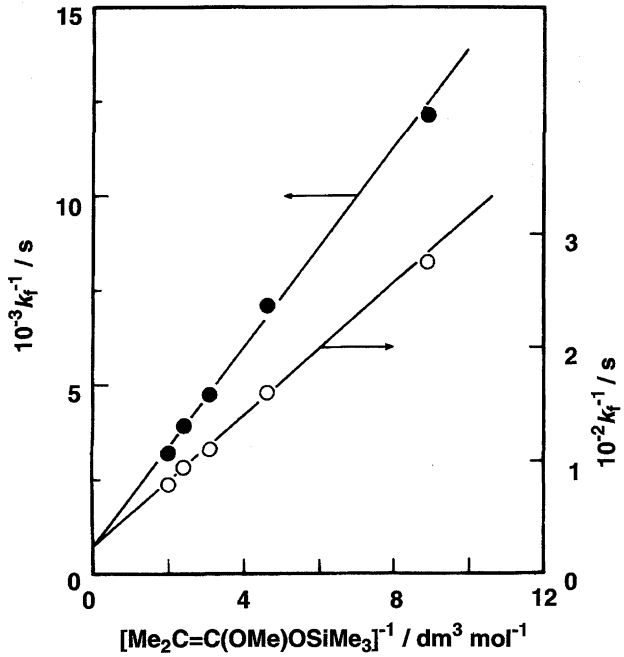

Fig. 5. Double reciprocal plots of the data in Fig. 4.

rate constant ($k_{obsd}=k_f/[\mathbf{1a}]$) under the experimental conditions that $K_{CT}[\mathbf{1a}]\ll1$ is a product $k_{obsd}=k_1K_{CT}$ or a simple bimolecular rate constant $k_{obsd}=k_2$. Unfortunately, however, the two processes are kinetically indistinguishable.[24] Nonetheless, the distinction may be made based on the nature of the activation step for the reaction as discussed below.

Electron Transfer vs. Nucleophilic Mechanisms. The observed second-order rate constant (k_{obsd}) generally decreases with a decrease in the one-electron reduction potential (E^0_{red}) of quinones. As such the highest reactivity is achieved for *o*-chloranil (E^0_{red}=0.14 V),[25] but no reaction takes place for chloro-*p*-benzoquinone (E^0_{red}=−0.34 V) and *p*-benzoquinone (E^0_{red}=−0.50 V).[10] Such a strong dependence of k_{obsd} on E^0_{red} suggests that electron transfer from **1a** to quinones is the rate-determining step for the addition of **1a** to quinones as shown representatively for the **1a**–*p*-chloranil system in Scheme 2. Electron transfer from **1a** to Cl_4Q in the CT complex gives the radical ion pair ($\mathbf{1a}^{\bullet+}Cl_4Q^{\bullet-}$). Since the spin of $\mathbf{1a}^{\bullet+}$ is mainly localized on the terminal carbon atom,[1] the carbon–oxygen bond may be formed before the cleavage of the Si–O bond to yield the carbon–oxygen adduct. Such a radical coupling process prior to the cleavage of the Si–O bond in $\mathbf{1a}^{\bullet+}$ has recently been reported for the addition of **1a** to C_{60} via photoinduced electron transfer.[26] However, the mechanism of the cleavage of the Si–O bond in $\mathbf{1a}^{\bullet+}$ and formation of the Si–O bond in the adduct with the quinone remains to be elucidated.

The rate constant of electron transfer in the EDA complex may be evaluated based on the Rehm–Weller Gibbs energy relation for electron transfer processes in Eq. 14,[27]

$$\Delta G^{\neq} = (\Delta G^0/2) + [(\Delta G^{\neq}_0)^2 + (\Delta G^0/2)^2]^{1/2} \qquad (14)$$

where ΔG^0 is the Gibbs energy change of electron transfer in the CT complex and $\Delta G^{\neq}_0$ is the intrinsic barrier of the

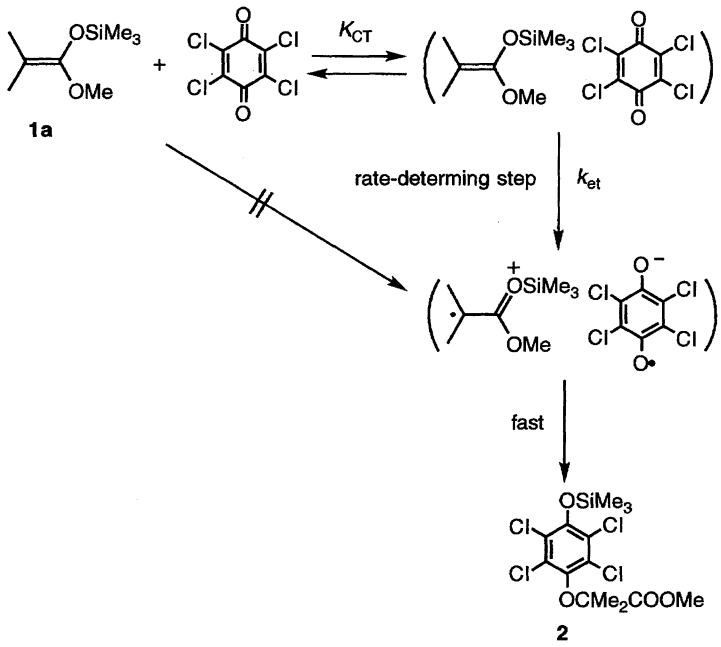

Scheme 2.

electron transfer reactions of **1a**. The ΔG^0 value may be given by Eq. 15,

$$\Delta G^0 = F(E^0_{ox} - E^0_{red}) + w_p \quad (15)$$

where the E^0_{ox} value of **1a** (0.90 V)[1] and the E^0_{red} values of quinones (Table 5) are known and the work term w_p which is required to bring the radical cation of **1a** and the quinone radical anion to the mean separation distance of the transition state. The w_p value for such a radical ion pair with opposite charge may be evaluated as ca. 0.1 eV although the w_p value is sensitive to the steric effect.[28] The $\Delta G^{\neq}_0$ value of **1a** has previously been reported as 5.2 kcal mol^{-1}.[1] By using these values the $\Delta G^{\neq}$ value can be evaluated as 19.6 kcal mol^{-1} for the **1a**–*p*-chloranil system, which is converted to the rate constant of intracomplex electron transfer (k_{et}) by using Eq. 16.

$$k_{et} = (kT/h)\exp(-\Delta G^{\neq}/RT) \quad (16)$$

The k_{et} value thus evaluated is 2.7×10^{-2} s^{-1} which agrees well with the observed k_1 value (4.4×10^{-2} s^{-1}) in Table 5. Although the k_{et} value was evaluated based on the energetics of electron transfer in acetonitrile which is more polar than dichloromethane in which the solvation energy of free ions and the Coulombic barrier to separation are greatly reduced compared to acetonitrile, the increase in the free energy change of electron transfer to produce free ions in dichloromethane may be largely canceled out by the increase in the Coulombic interaction in the radical ion pair in dichloromethane as compared with that in acetonitrile, as demonstrated in the case of photoaddition of ketene silyl acetals to the triplet excited state of 10-methylacridone in benzene.[29] Thus, the agreement between the k_{et} and k_{obsd} values supports the electron transfer mechanism through the EDA complex in Scheme 2.

The reactivities of various ketene silyl acetals towards *p*-fluoranil, *p*-chloranil, and *p*-bromanil are compared in Table 6 where the one-electron oxidation potentials of ketene silyl acetals are also listed for comparison. The k_{obsd} values of another β,β-dimethyl-substituted ketene silyl acetal (**1b**) are similar to those of **1a**. In the case of monomethyl-substituted ketene silyl acetal (**1c**) and nonsubstituted ketene silyl acetal (**1d**), however, the k_{obsd} values are significantly larger than those of **1a** except for the **1c**–*p*-fluoranil system despite the much higher one-electron oxidation potentials (Table 6). The

Table 6. Rate Constants for Addition of Various Ketene Silyl Acetals to *p*-Fluoranil, *p*-Chloranil, and *p*-Bromanil in CH_2Cl_2 at 298 K

Ketene silyl acetal	E^0_{ox} [a] vs. SCE/V	k_{obsd}/dm^3 mol^{-1} s^{-1} F$_4$Q	Cl$_4$Q	Br$_4$Q
$Me_2C{=}C(OMe)OSiMe_3$	0.90	4.4×10^{-1}	3.5×10^{-2}	7.4×10^{-3}
$Me_2C{=}C(OEt)OSiEt_3$	0.87	5.1×10^{-1}	2.4×10^{-2}	5.4×10^{-3}
(*E*)-Me(H)C=C(OEt)OSiEt$_3$	1.05	3.9×10^{-1}	2.9×10^{-1}	1.3×10^{-1}
$H_2C{=}C(OEt)OSiEt_3$	1.30	5.8	2.6×10^{-2}	1.2×10^{-2}
$Me_3Si(H)C{=}C(OMe)OSiMe_3$	b)	8.2×10^{-2}	2.0×10^{-4}	c)

a) Taken from Ref. 1. b) Not reported. c) The reaction was too slow to determine k_{obsd} accurately.

k_{et} value of **1d** would be reduced by 10^8 times as compared to **1a** based on Eqs. 14, 15, and 16. However, the k_{obsd} values of **1d** are even much larger than those of **1a** except for the case of *p*-chloranil. In such a case the nucleophilic attack of ketene silyl acetals to the positively charged carbonyl carbon of *p*-chloranil may dominate as compared to the electron transfer process in Scheme 2, yielding the carbon–carbon adduct (Eq. 3) rather than the carbon–oxygen adduct.

Magnesium Ion-Catalyzed Electron Transfer. It has recently been found that Mg^{2+} forms the 1 : 1 and 2 : 1 complexes with the radical anion of *p*-benzoquinone (Q) as shown in Eqs. 17 and 18,

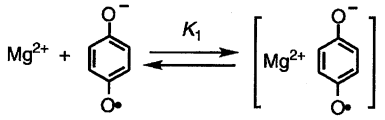

(17)

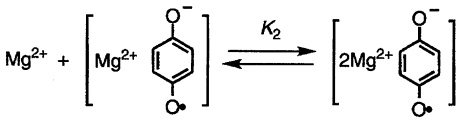

(18)

where K_1 and K_2 are the formation constants of Mg^{2+}–$Q^{\bullet-}$ and $2Mg^{2+}$–$Q^{\bullet-}$ complexes, respectively.[13] The formation constant K_2 of the 2 : 1 complex of $Q^{\bullet-}$ has been determined as 4.5 $dm^3\ mol^{-1}$ in MeCN at 298 K by the direct detection of the transient absorption spectra as well as the ESR spectra of the Mg^{2+}–$Q^{\bullet-}$ and $2Mg^{2+}$–$Q^{\bullet-}$ complexes.[13] The kinetic expression of the Mg^{2+} catalysis changes from the first-order to second-order in $[Mg^{2+}]$ under the conditions that Mg^{2+} forms the 2 : 1 complexes with the corresponding radical anions.[13] On the other hand, it has been confirmed that no 2 : 1 complex formation occurs with the oxidized form of *p*-benzoquinone derivatives with Mg^{2+}; they can form, if any, only the 1 : 1 complexes.[13] Thus, the examination of the catalytic effects of Mg^{2+} (vide infra) provides a valuable mechanistic insight into the contribution of electron transfer processes.

No reaction takes place between **1a** and *p*-benzoquinone in MeCN, the electron affinity of which is significantly smaller than that of *p*-chloranil (vide supra). In the presence of magnesium perchlorate, however, the reduction of *p*-benzoquinone and its derivatives by **1a** occurs efficiently in MeCN. The kinetic expression of the Mg^{2+} catalysis changes from the first-order to second-order in $[Mg^{2+}]$ under the conditions that Mg^{2+} forms the 2 : 1 complexes with the corresponding radical anions as shown in Fig. 6.[13] A quantitative evaluation of the contribution of the Mg^{2+}-catalyzed electron transfer process on the reduction of Q by **1a** may be achieved by analyzing the dependence of k_{obsd} on $[Mg^{2+}]$ as follows.

The one-electron reduction potential of Q in the presence of Mg^{2+} may be shifted to the positive direction by the formation of the Mg^{2+} complexes of $Q^{\bullet-}$ (Eqs. 17 and 18). Since the oxidized electroactive species is [Q] and the reduced electroactive species is $[Q^{\bullet-}]+[Mg^{2+}\text{–}Q^{\bullet-}]+[2Mg^{2+}\text{–}Q^{\bullet-}]$, where $[Mg^{2+}\text{–}Q^{\bullet-}]=K_1[Mg^{2+}][Q^{\bullet-}]$ and $[2Mg^{2+}\text{–}Q^{\bullet-}]=K_1K_2[Mg^{2+}]^2[Q^{\bullet-}]$, the expression for the

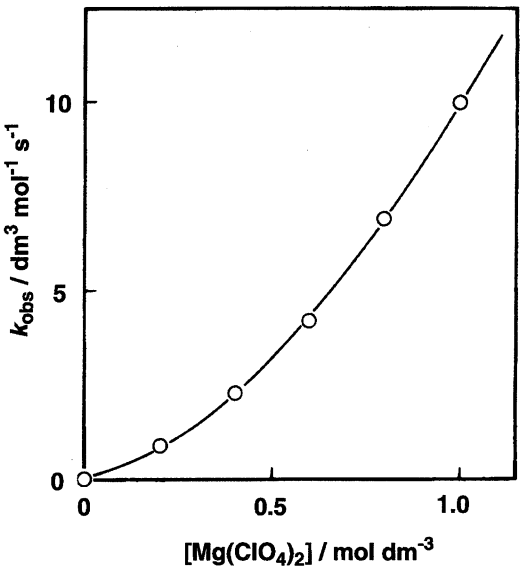

Fig. 6. Plot of the observed second-order rate constants (k_{obsd}) vs. $[Mg(ClO_4)_2]$ for the reduction of *p*-benzoquinone (7.6×10^{-4} mol dm^{-3}) by **1a** (9.2×10^{-2} mol dm^{-3}) in MeCN at 298 K.

Nernst equation of the one-electron reduction potential in the presence of Mg^{2+} (E_{red}) may be given by Eq. 19.[30,31]

$$E_{red} = E^0_{red} + (2.3RT/F)\ \log(1 + K_1[Mg^{2+}] + K_1K_2[Mg^{2+}]^2) \quad (19)$$

Thus, by replacing E^0_{red} in Eq. 15 by E_{red} in Eq. 19 is derived the kinetic expression of the observed second-order rate constant (k_{obsd}) with respect to $[Mg^{2+}]$ as given by Eq. 20,

$$k_{obsd} = k_0(1 + K_1[Mg^{2+}] + K_1K_2[Mg^{2+}]^2) \quad (20)$$

where $k_0=Z\exp(-F(E^0_{ox}+w_p)/RT)$. Under the conditions that $K_1[Mg^{2+}]\gg1$, Eq. 20 is reduced to Eq. 21,

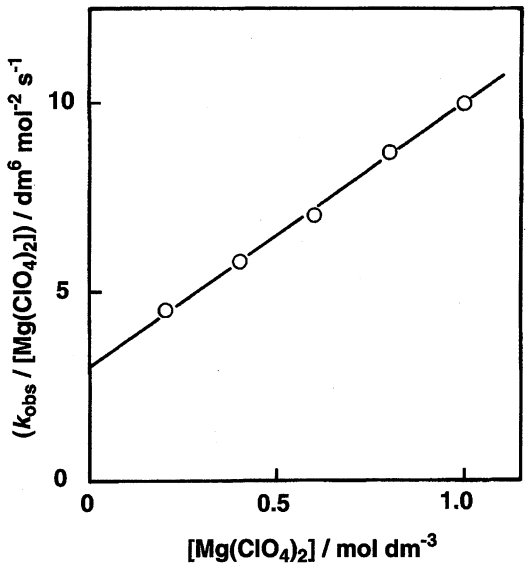

Fig. 7. Plot of $k_{obsd}/[Mg(ClO_4)_2]$ vs. $[Mg(ClO_4)_2]$ for the reduction of *p*-benzoquinone by **1a** in the presence of $Mg(ClO_4)_2$ in MeCN at 298 K.

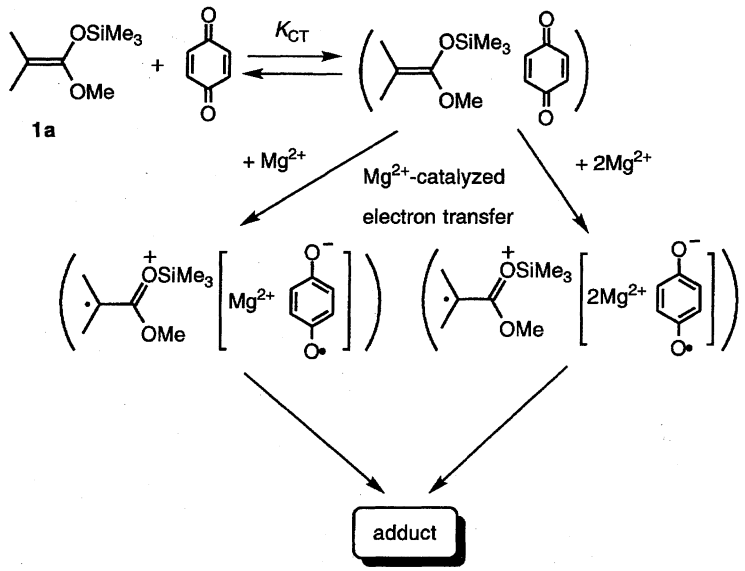

Scheme 3.

$$k_{obsd}/[Mg^{2+}] = k_0K_1(1 + K_2[Mg^{2+}]) \quad (21)$$

which predicts a linear correlation between $k_{obsd}/[Mg^{2+}]$ and $[Mg^{2+}]$. Such a correlation is verified experimentally as shown in Fig. 7, where $k_{obsd}/[Mg^{2+}]$ is plotted against $[Mg^{2+}]$. Moreover, from the slope and intercept is obtained the formation constant of $2Mg^{2+}$–$Q^{\bullet-}$ as 2.1. Although the K_2 value derived by using Eq. 21 is somewhat smaller than the K_2 value (4.5) derived directly from the detection of the transient spectra of the Mg^{2+} complexes of $Q^{\bullet-}$,[13] the reasonable agreement between two independent methods strongly indicates the important contribution of Mg^{2+}-catalyzed electron transfer processes in the two-electron redox reactions of *p*-benzoquinone by **1a** as shown in Scheme 3. In the case of *p*-chloranil the reduction by **1a** occurs in the absence of Mg^{2+} (Eq. 1). In the presence of Mg^{2+}, the rate increases linearly with an increase in $[Mg^{2+}]$ as shown in Fig. 8, where no second-order dependence is observed. In the case of *p*-chloranil, it has been confirmed that no 2 : 1 complex between Mg^{2+} and the *p*-chloranil radical anion is formed under the experimental conditions in Fig. 8. Thus, the catalytic effect of Mg^{2+} in the case of *p*-chloranil, only the 1 : 1 complex between Mg^{2+} and the radical anion may be involved in the Mg^{2+}-catalyzed electron transfer process which is the rate-determining step for the addition of **1a** to *p*-chloranil.

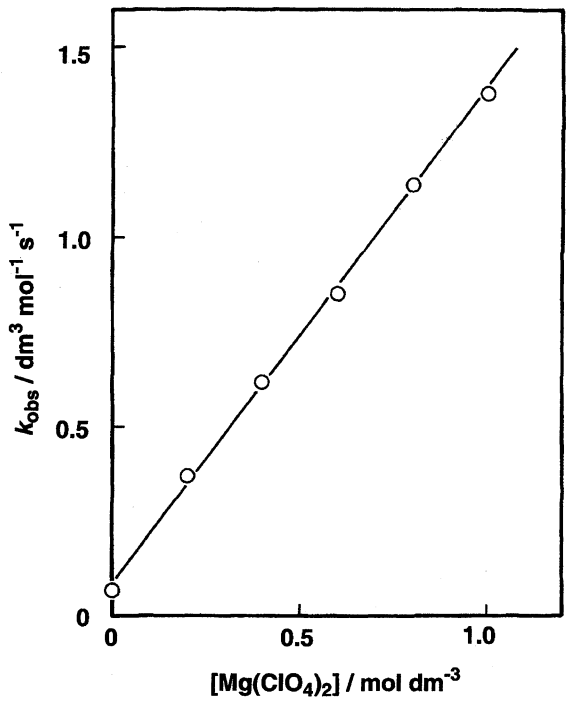

Fig. 8. Plot of the observed second-order rate constants (k_{obsd}) vs. $[Mg(ClO_4)_2]$ for the reduction of *p*-chloranil (5.0×10^{-4} mol dm^{-3}) by **1a** in MeCN at 298 K.

References

1) S. Fukuzumi, M. Fujita, J. Otera, and Y. Fujita, *J. Am. Chem. Soc.*, **114**, 10271 (1992).

2) T. Sato, Y. Wakahara, J. Otera, H. Nozaki, and S. Fukuzumi, *J. Am. Chem. Soc.*, **113**, 4028 (1991); J. Otera, Y. Fujita, T. Sato, H. Nozaki, S. Fukuzumi, and M. Fujita, *J. Org. Chem.*, **57**, 5054 (1992).

3) N. Kornblum, *Angew. Chem., Int. Ed. Engl.*, **14**, 734 (1975); S. F. Martin, *Tetrahedron*, **36**, 419 (1980).

4) M. T. Reetz, K. Schwellnus, F. Hübner, W. Massa, and R. E. Schmidt, *Chem. Ber.*, **116**, 3708 (1983); G. E. Totten, G. Wenke, and Y. E. Rhodes, *Synth. Commun.*, **15**, 291 (1985); R. Rathore, Z. Lin, and J. K. Kochi, *Tetrahedron Lett.*, **34**, 1859 (1993); T. M. Bockman, S. Perrier, and J. K. Kochi, *J. Chem. Soc., Perkin Trans. 2*, **1993**, 595.

5) K. Narasaka, N. Arai, and T. Okauchi, *Bull. Chem. Soc. Jpn.*, **66**, 2995 (1993); K. Narasaka and Y. Kohno, *Bull. Chem. Soc. Jpn.*, **66**, 3456 (1993); Y. Kohno and K. Narasaka, *Bull. Chem. Soc. Jpn.*, **68**, 322 (1995); E. Baciocchi, A. Casu, and R. Ruzziconi, *Tetrahedron Lett.*, **28**, 3707 (1989).

6) A. Bhattacharya, L. M. DiMichele, U.-H. Dolling, E. J. J. Grabowski, and V. J. Grenda, *J. Org. Chem.*, **54**, 6118 (1989).

7) A. Pross and S. S. Shaik, *Acc. Chem. Res.*, **16**, 363 (1983);

A. Pross, *Acc. Chem. Res.*, **18**, 212 (1985); S. S. Shaik, *Prog. Phys. Org. Chem.*, **15**, 197 (1985); J. K. Kochi, *Angew. Chem., Int. Ed. Engl.*, **27**, 1227 (1988); J.-M. Mattalia, B. Vacher, A. Samat, and M. Chanon, *J. Am. Chem. Soc.*, **114**, 4111 (1992).

8) U. Eisner and J. Kuthan, *Chem. Rev.*, **72**, 1 (1972); D. M. Stout and A. I. Meyers, *Chem. Rev.*, **82**, 223 (1982).

9) S. Fukuzumi, "Advances in Electron Transfer Chemistry," ed by P. S. Mariano, JAI Press, Greenwich (1992), Vol. 2, p. 65; S. Fukuzumi and T. Tanaka, "Photoinduced Electron Transfer," ed by M. A. Fox and M. Chanon, Elsevier, Amsterdam (1988), Part C, Chap. 10.

10) S. Fukuzumi, S. Koumitsu, K. Hironaka, and T. Tanaka, *J. Am. Chem. Soc.*, **109**, 305 (1987), and references cited therein.

11) J. W. Bunting, *Bioorg. Chem.*, **19**, 456 (1991), and references cited therein.

12) S. Fukuzumi, N. Nishizawa, and T. Tanaka, *J. Chem. Soc., Perkin Trans. 2*, **1985**, 371.

13) S. Fukuzumi and T. Okamoto, *J. Am. Chem. Soc.*, **115**, 11600 (1993); S. Fukuzumi and T. Okamoto, *J. Chem. Soc., Chem. Commun.*, **1994**, 521.

14) A preliminary report has appeared; S. Fukuzumi, M. Fujita, G. Matsubayashi, and J. Otera, *Chem. Lett.*, **1993**, 1451.

15) R. E. Ireland, P. Wipf, and J. D. Armstrong, III, *J. Org. Chem.*, **56**, 650 (1991); C. Gennari, M. G. Beretta, A. Bernardi, G. Moro, C. Scolastico, and R. Todeschini, *Tetrahedron*, **42**, 893 (1986); J. Otera, Y. Fujita, and S. Fukuzumi, *Synlett*, **1994**, 213.

16) D. D. Perrin, W. L. F. Armarego, and D. R. Perrin, "Purification of Laboratory Chemicals," Pergamon Press, Elmsford (1966).

17) C. T. North, D. C. Phillips, and F. C. Matheus, *Acta Crystallogr., Sect. A*, **24A**, 351 (1968).

18) M. Main, S. E. Hull, L. Lessinger, G. Germain, J.-P. Declercq, and M. M. Woolfson, "A System of Computer Programs of Crystal Structures from X-Ray Diffraction Data, MULTAN 78," University of York (1978).

19) "International Tables for X-Ray Crystallography," Kynoch Press, Birminbham (1974), Vol. 4.

20) R. Foster, "Organic Charge Transfer Complexes," Academic Press, New York (1969); R. Foster, "Molecular Complexes," Crane Russak and Co., New York (1974), Vol. 2, p. 108.

21) H. A. Benesi and J. H. Hildebrand, *J. Am. Chem. Soc.*, **71**, 2703 (1949).

22) S. Fukuzumi and J. K. Kochi, *J. Phys. Chem.*, **85**, 648 (1981).

23) R. C. Larson, R. T. Iwamoto, and R. N. Adams, *Anal. Chim. Acta*, **25**, 371 (1961). The value of C_a for the SCE reference in MeCN is 4.40 V.

24) S. Fukuzumi and J. K. Kochi, *J. Am. Chem. Soc.*, **102**, 2141 (1980).

25) D. H. Evans, "Encyclopedia of Electrochemistry of the Elements, Organic Section," ed by A. J. Bard and H. Lund, Marcel Dekker, New York (1978), Chap. XII-1, and references cited therein.

26) K. Mikami, S. Matsumoto, A. Ishida, S. Takamuku, T. Suenobu, and S. Fukuzumi, *J. Am. Chem. Soc.*, **117**, 11134 (1995).

27) A. Rehm and A. Weller, *Isr. J. Chem.*, **8**, 259 (1970).

28) S. Fukuzumi, C. L. Wong, and J. K. Kochi, *J. Am. Chem. Soc.*, **102**, 2928 (1980).

29) S. Fukuzumi, M. Fujita, and J. Otera, *J. Org. Chem.*, **58**, 5405 (1993).

30) L. Meites, "Polarographic Techniques," 2nd ed, Wiley, New York (1965), pp. 203—301.

31) S. Fukuzumi, K. Ishikawa, K. Hironaka, and T. Tanaka, *J. Chem. Soc., Perkin Trans. 2*, **1987**, 751.